Dynamic Modeling of Doubly Fed Induction Generator Wind Turbines

Janaka B. Ekanayake, *Senior Member, IEEE*, Lee Holdsworth, XueGuang Wu, and Nicholas Jenkins, *Senior Member, IEEE*

***Abstract*—It is now recognized that many large wind farms will employ doubly fed induction generator (DFIG) variable speed wind turbines. A number of such wind farms are already in operation and more are planned or under construction. With the rising penetration of wind power into electricity networks, increasingly comprehensive studies are required to identify the interaction between the wind farm(s) and the power system. These require accurate models of doubly fed induction generator wind turbines and their associated control and protection circuits. A dynamic model has been derived, which can be used to simulate the DFIG wind turbine using a single-cage and double-cage representation of the generator rotor, as well as a representation of its control and protection circuits. The model is suitable for use in transient stability programs that can be used to investigate large power systems. The behavior of a wind farm and the network under various system disturbances was studied using this dynamic model. The influence of the DFIG control on the stability of the wind farm was also investigated by considering different control gains and by applying network voltage control through both stator side and rotor side converters.**

***Index Terms*—Doubly fed induction generators, power system dynamic stability, power system modeling.**

NOMENCLATURE

v_s	Stator voltage.
v_r	Rotor voltage.
i_s, i_r	Stator and rotor current.
R_s, R_r, R_d	Stator, rotor,and double-cage machine resistance.
ω_s, ω_r	Synchronous and rotor angular frequency.
λ	Flux linkage.
L_m	Magnetizing inductance.
L_{rm}	Mutual inductance between two rotor coils.
L_s, L_r, L_d	Stator, rotor, and double-cage leakage inductance.
L_{ss}, L_{rr}, L_{dd}	Stator, rotor, and double-cage self inductance.
s	Rotor slip.
J	Moment of inertia of entire wind turbine.
T_m, T_e, T_{sp}	Mechanical, electromagnetic, set point torque.
T_{opt}	Optimal torque.
K_{opt}	Optimal torque/speed constant of the wind turbine.
p	d/dt
$-$	Superscript indicates a per unit quantity.
d,q	First subscript indicates direct and quadrature axes quantities.
s,r ,d	Second subscript indicates stator, rotor, and double-cage.

Manuscript received October 23, 2002. This work was supported in part by the Association of Commonwealth Universities, EPSRC. and in part by the Tyndall Centre for Climatic Change Research.

J. B. Ekanayake is with the Department of Electrical and Electronics Engineering and the University of Peradeniya, Sri Lanka, 20400, and the Tyndall Centre for Climate Change Research, Norwich, NR4 7TJ, U.K. (e-mail: jbe@ee.pdn.ac.lk)

L. Holdsworth, X.G. Wu, and N. Jenkins are with The Manchester Centre for Electrical Energy, University of Machester Institute and Technology, U.K. and the Tyndall Centre for Climate Change Research, Norwich, NR4 7TJ, U.K. (e-mail: l.holdsworth@umist.ac.uk; w.xueguang@umist.ac.uk; n.jenkins@umist.ac.uk).

Digital Object Identifier 10.1109/TPWRS.2003.811178

I. INTRODUCTION

MANY countries have now recognized the wind as a sustainable source of energy and the installed capacity of wind generation worldwide now exceeds 25 GW. Both for reasons of network compatibility and to reduce mechanical loads, many large wind turbines (installed either offshore or onshore) will operate at variable speed and use doubly fed induction generators (DFIGs). [1]

In the past, most national network design codes and standards did not require wind farms to support the power system during a disturbance. For example during a network fault or sudden drop in frequency wind turbines were tripped off the system. However, with the increased use of wind energy, wind farms will have to continue to operate during system disturbances and support the network voltage and frequency. Network design codes are now being revised to reflect this new requirement. Therefore,it is necessary to carry out simulation studies to understand the impact of system disturbances on wind turbines and consequently on the power system itself. These studies require accurate steady state and dynamic models of wind turbines and their associated control and protection.

Reduced order models of DFIG wind turbines for dynamic studies have been published [2]–[4]. These models are based on a single-cage representation of the rotor. For correct representation of the DFIG wind turbine, it is important to model the control system used. In [2] and [3], it was assumed that the d-axis coincides with the maximum of the stator flux (this assumption leads to difficulties when initializing the dynamic model from a power system load flow) and the papers give only limited details of the control system used. In [4], no information of the controller used is given.

It has long been recognized that in order to represent an induction machine under system disturbances such as a fault, it is

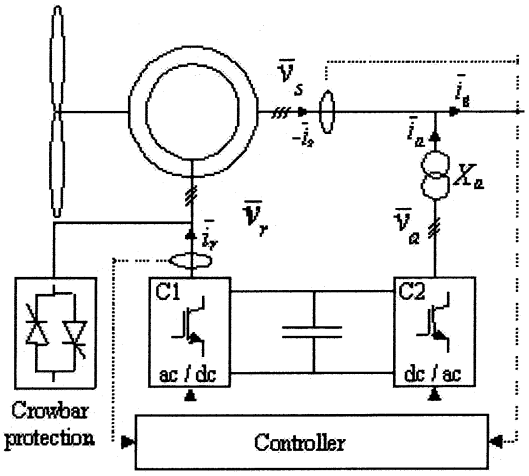

Fig. 1. Basic configuration of a DFIG wind turbine.

desirable to use a double-cage model, which represents the transient and subtransient behavior of the machine more accurately [5]. This paper presents a model that can be used for single-cage and double-cage representation of the DFIG and its control and protection circuits.

II. Modeling of the DFIG

DFIG wind turbines utilize a wound rotor induction generator, where the rotor winding is fed through back-to-back variable frequency, voltage source, converters [1], [2]. A typical configuration of a DFIG–based wind turbine is shown schematically in Fig. 1. The machine and converters are protected by voltage limits and an over-current "crowbar" circuit. The converter system enables variable speed operation of the wind turbine by decoupling the power system electrical frequency and the rotor mechanical frequency. A more detailed description of the DFIG system together with its control and protection circuits can be found in [6].

A. Machine Modeling

The generalized reduced order machine model was developed based on the following conditions and assumptions.

a) The stator current was assumed positive when flowing toward the machine.
b) The equations were derived in the synchronous reference frame using direct (d) and quadrature (q) axis representation [7], [8].
c) The q-axis was assumed to be 90° ahead of the d-axis in the direction of rotation.
d) The q component of the stator voltage used within the model is chosen to be equal to the real part of the generator busbar voltage obtained from the load flow solution that is used to initialize the model.
e) The dc component of the stator transient current was ignored, permitting representation of only fundamental frequency components.
f) The higher order harmonic components in the rotor injected voltages are neglected.

The reduced order machine model in per unit was obtained as

$$\begin{cases} \overline{v}_{ds} = \overline{R}_s \times \bar{i}_{ds} - \overline{\lambda}_{qs} \\ \overline{v}_{qs} = \overline{R}_s \times \bar{i}_{qs} + \overline{\lambda}_{ds} \end{cases} \tag{1}$$

$$\begin{cases} \overline{v}_{dr} = \overline{R}_r \times \bar{i}_{dr} - s \times \overline{\lambda}_{qr} + \frac{1}{\omega_s}\frac{d}{dt}\overline{\lambda}_{dr} \\ \overline{v}_{qr} = \overline{R}_r \times \bar{i}_{qr} + s \times \overline{\lambda}_{dr} + \frac{1}{\omega_s}\frac{d}{dt}\overline{\lambda}_{qr} \end{cases} \tag{2}$$

$$\begin{cases} \overline{v}_{dd} = \overline{R}_d \times \bar{i}_{dd} - s \times \overline{\lambda}_{qd} + \frac{1}{\omega_s}\frac{d}{dt}\overline{\lambda}_{dd} = 0 \\ \overline{v}_{qd} = \overline{R}_d \times \bar{i}_{qd} + s \times \overline{\lambda}_{dd} + \frac{1}{\omega_s}\frac{d}{dt}\overline{\lambda}_{qd} = 0 \end{cases} \tag{3}$$

where

$$\begin{bmatrix} \overline{\lambda}_{ds} \\ \overline{\lambda}_{dr} \\ \overline{\lambda}_{dd} \end{bmatrix} = \begin{bmatrix} \overline{L}_{ss} & \overline{L}_m & \overline{L}_m \\ \overline{L}_m & \overline{L}_{rr} & \beta\overline{L}_m \\ \overline{L}_m & \beta\overline{L}_m & \overline{L}_{dd} \end{bmatrix} \begin{bmatrix} \bar{i}_{ds} \\ \bar{i}_{dr} \\ \bar{i}_{dd} \end{bmatrix} \tag{4}$$

and

$$\begin{bmatrix} \overline{\lambda}_{qs} \\ \overline{\lambda}_{qr} \\ \overline{\lambda}_{qd} \end{bmatrix} = \begin{bmatrix} \overline{L}_{ss} & \overline{L}_m & \overline{L}_m \\ \overline{L}_m & \overline{L}_{rr} & \beta\overline{L}_m \\ \overline{L}_m & \beta\overline{L}_m & \overline{L}_{dd} \end{bmatrix} \begin{bmatrix} \bar{i}_{qs} \\ \bar{i}_{qr} \\ \bar{i}_{qd} \end{bmatrix}. \tag{5}$$

In (4) and (5)

$$\beta = 1 + \frac{\overline{L}_{rm}}{\overline{L}_m}, \quad \overline{L}_{ss} = \overline{L}_s + \overline{L}_m,$$
$$\overline{L}_{rr} = \overline{L}_r + \beta\overline{L}_m \quad \text{and} \quad \overline{L}_{dd} = \overline{L}_d + \beta\overline{L}_m.$$

From (4) and (5), the stator current can be derived in the per unit form as

$$\begin{cases} \bar{i}_{ds} = \left(\frac{\overline{\lambda}_{ds} - \overline{L}_m \times \bar{i}_{dr} - \overline{L}_m \times \bar{i}_{dd}}{\overline{L}_{ss}}\right) = \frac{\overline{v}_{qs}}{\overline{L}_{ss}} - \frac{\overline{L}_m}{\overline{L}_{ss}}\bar{i}_{dr} - \frac{\overline{L}_m}{\overline{L}_{ss}}\bar{i}_{dd} \\ \bar{i}_{qs} = \left(\frac{\overline{\lambda}_{qs} - \overline{L}_m \times \bar{i}_{qr} - \overline{L}_m \times \bar{i}_{qd}}{\overline{L}_{ss}}\right) = -\frac{\overline{v}_{ds}}{\overline{L}_{ss}} - \frac{\overline{L}_m}{\overline{L}_{ss}}\bar{i}_{qr} - \frac{\overline{L}_m}{\overline{L}_{ss}}\bar{i}_{qd} \end{cases}. \tag{6}$$

$$\begin{cases} p\bar{i}_{dr} = \frac{\overline{X}_3}{\sigma_1}\overline{v}_{dr} - \frac{\overline{R}_r\overline{X}_3}{\sigma_1}\bar{i}_{dr} + \frac{\overline{R}_d\overline{X}_2}{\sigma_1}\bar{i}_{dd} + s\omega_s\bar{i}_{qr} + \frac{\overline{L}_m}{\overline{L}_{ss}}\sigma_2\left[s\overline{v}_{ds} + \frac{1}{\omega_s}p\overline{v}_{qs}\right] \\ p\bar{i}_{qr} = \frac{\overline{X}_3}{\sigma_1}\overline{v}_{qr} - \frac{\overline{R}_r\overline{X}_3}{\sigma_1}\bar{i}_{qr} + \frac{\overline{R}_d\overline{X}_2}{\sigma_1}\bar{i}_{qd} - s\omega_s\bar{i}_{dr} + \frac{\overline{L}_m}{\overline{L}_{ss}}\sigma_2\left[s\overline{v}_{qs} - \frac{1}{\omega_s}p\overline{v}_{ds}\right] \\ p\bar{i}_{dd} = -\frac{\overline{X}_2}{\sigma_1}\overline{v}_{dr} + \frac{\overline{R}_r\overline{X}_2}{\sigma_1}\bar{i}_{dr} - \frac{\overline{R}_d\overline{X}_1}{\sigma_1}\bar{i}_{dd} + s\omega_s\bar{i}_{qd} + \frac{\overline{L}_m}{\overline{L}_{ss}}\sigma_3\left[s\overline{v}_{ds} + \frac{1}{\omega_s}p\overline{v}_{qs}\right] \\ p\bar{i}_{qd} = -\frac{\overline{X}_2}{\sigma_1}\overline{v}_{qr} + \frac{\overline{R}_r\overline{X}_2}{\sigma_1}\bar{i}_{qr} - \frac{\overline{R}_d\overline{X}_1}{\sigma_1}\bar{i}_{qd} - s\omega_s\bar{i}_{dd} + \frac{\overline{L}_m}{\overline{L}_{ss}}\sigma_3\left[s\overline{v}_{qs} - \frac{1}{\omega_s}p\overline{v}_{ds}\right] \end{cases}. \tag{7}$$

Using (2) to (5), the rotor currents can be derived in the following per unit form. See (7) at the bottom of the previous page where

$$\overline{X}_1 = \left[\overline{L}_{rr} - \frac{\overline{L}_m^2}{\overline{L}_{ss}}\right], \quad \overline{X}_2 = \left[\beta\overline{L}_m - \frac{\overline{L}_m^2}{\overline{L}_{ss}}\right],$$
$$\overline{X}_3 = \left[\overline{L}_{dd} - \frac{\overline{L}_m^2}{\overline{L}_{ss}}\right],$$
$$\sigma_1 = \frac{\overline{X}_1\overline{X}_3 - \overline{X}_2^2}{\omega_s}, \quad \sigma_2 = \left[\frac{\overline{X}_2 - \overline{X}_3}{\sigma_1}\right]$$
$$\text{and} \quad \sigma_3 = \left[\frac{\overline{X}_2 - \overline{X}_1}{\sigma_1}\right].$$

The per unit electromagnetic torque (positive for a motor) is calculated using

$$T_e = \overline{\lambda}_{ds} \times \overline{i}_{qs} - \overline{\lambda}_{qs} \times \overline{i}_{ds} = \overline{v}_{qs}\overline{i}_{qs} + \overline{v}_{ds}\overline{i}_{ds}. \tag{8}$$

Finally, if T_m is the mechanical torque, which depends upon wind speed, the machine swing equation is given by

$$\frac{d\omega_r}{dt} = \frac{1}{J} \times (T_m - T_e). \tag{9}$$

Equation (9), of course, represents the wind turbine as a single lumped inertia. It has been shown by others [9] that for some studies, it is important to represent the dynamics of the wind turbine mechanical drive train using a multiple mass model. If this is required, (9) may be expanded, as shown in [9], to include the masses of the generator, gearbox, and blades with the associated torsional stiffnesses and damping.

Equations (6) – (9) were used to obtain the reduced order dynamic model of the DFIG.

B. Modeling of the DFIG Converters and Control System

For the model, it was assumed that the converters are ideal and the dc link voltage between the converters is constant. This decouples converter C2 from C1. Converter C1 was modeled as a voltage source whereas converter C2 was modeled as a current source.

The rotor speed was controlled by v_{qr} which is the q-component of the injected voltage, through converter C1. The control scheme used for speed control is shown in Fig. 2. The optimum torque – speed curve shown in the figure was used as the reference for generator torque demand. This curve was mainly characterized by three sections namely: (a) an optimal characteristic curve given by $T_{opt} = K_{opt}\omega_r^2$ (where ω_r is the measured rotor speed) in between the cut-in wind speed and speed limit, (b) a constant speed characteristic up to the rated torque, and (c) a constant power characteristic beyond the speed limit followed by blade pitch control action for high wind speeds. The set point torque corresponding to the speed of the machine was translated into i_{qr} using the block "$\Re$" where the function $\Re$ is given by the following equation:

$$\Re = \frac{\overline{L}_{ss}}{\overline{L}_m\overline{v}_{qs}}\left[T_{sp} + \overline{v}_{ds}\overline{i}_{ds}\right] - \frac{\overline{v}_{ds}}{\overline{L}_m} - \overline{i}_{qd}. \tag{10}$$

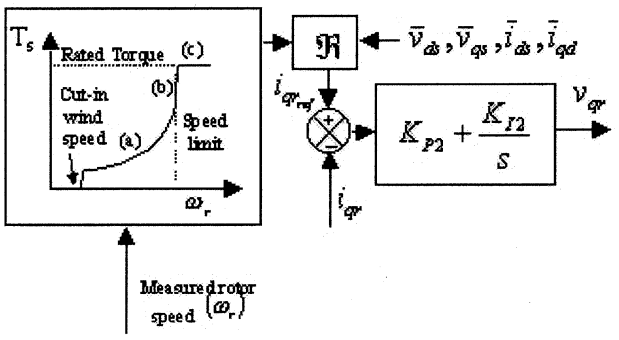

Fig. 2. Speed control scheme of the DFIG.

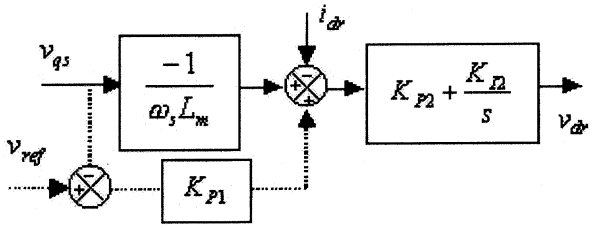

Fig. 3. No load PFC and VC through C1 for the DFIG.

The current error (the difference between the desired and achieved i_{qr}) together with a PI controller was used to obtain v_{qr}.

The d-component of the converter C_1 voltage v_{dr} was used for compensation for the generator magnetizing reactive power (No load PFC) as shown in Fig. 3. An outer loop (shown in dotted lines) was introduced for the voltage control (VC) through converter C_1. The VC through converter C_2 was introduced by comparing v_{qs} with a reference voltage v_{ref} and the error was regulated through a PI controller to obtain the current $\overline{i}_a$ required to be added to the generator output current $\overline{i}_s$ as shown in Fig. 1.

An alternative approach would be to use a current control converter for C1, thus the rotor current can be tracked directly. However simulating this control technique would require significant modifications to the machine model given in (7).

C. Modeling of the DFIG Protection

The controller model of the DFIG system included rotor voltage and current limits. The limits were selected depending on the megawatt capacity of the generator and the rating of the converters. Converter C1 was protected against over-current on the rotor circuits by a "single-shot crowbar," as shown in Fig. 1. The operation of the crowbar was modeled by deactivating the converters upon the detection of rotor current magnitude above the current protection limit and short-circuiting the generator rotor.

III. Double Fed Induction Machine Under Faults

A. Fault Current Contribution

Consider a fixed speed induction generator (FSIG) in which, immediately after a fault occurs, the stator voltage and flux reduces toward zero. The voltage drop depends, of course, on the location of the fault. The rotor current then increases to attempt

to maintain the flux linkage within the rotor windings constant [10]. However, for a DFIG the increase in the rotor current immediately after a fault will be determined by two factors. The first is the change in the stator flux and the second is the change in the rotor injected voltage.

According to Figs. 2 and 3 and (10), for a given mechanical torque and speed $|i_{dr_{ref}}| \propto |v_{qs}|$ and $|i_{qr_{ref}}| \propto 1/|v_{qs}|$. Therefore, as a fault occurs $|i_{dr_{ref}}|$ decreases and $|i_{qr_{ref}}|$ increases. These changes will reflect on the controllers, thus changing $|v_{dr}|$ and $|v_{qr}|$. The magnitude of the change acts directly through the proportional gain of the controller. The change in the rotor voltage components has a direct impact on the rate of change of the rotor current components due to the inductive nature of the rotor circuit (see (7)). In Figs. 2 and 3, the operation of the controllers results in a change in the injected voltages that oppose the sudden increase in the rotor current.

The following two operating conditions were simulated, by changing the controller gains.

1) The proportional gain of the controller was set to a low value. The increase in the rotor current triggered the crowbar, thus interrupting the operation of the DFIG. In practice, this would result in the turbine circuit breaker being opened and the wind turbine being braked to a standstill.
2) The proportional gain of the controller was set to a high value. The rotor current was then less than the current limit, thus ensuring continuous operation of the DFIG during the fault.

If the crowbar is not triggered at the inception of the fault and the wind turbine continues to operate then during the fault, V_{qs} remains low but nearly constant. Therefore, $|i_{dr_{ref}}|$ and $|i_{qr_{ref}}|$ are also nearly constant and depending on the speed of response and gains of the controller, both $|i_{dr}|$ and $|i_{qr}|$ start to follow their respective reference inputs.

While the flux within the machine and injected rotor voltages play a key role, the imbalance between the mechanical power and electrical power also contributes to the machine operation under a fault as in the case of a FSIG.

B. Behavior at Fault Clearance

During the fault, the stator voltage and rotor flux have been reduced, the injected rotor voltage has been changed and the rotor speed has been increased. Immediately the fault is cleared the stator voltage is restored, and the demagnetized stator and rotor oppose this change in flux thus leading to an increase in the rotor and stator currents. However, restoration of the stator voltage changes $|i_{dr_{ref}}|$ and $|i_{qr_{ref}}|$, and immediately the fault is cleared $|i_{qr}| \rangle |i_{qr_{ref}}|$ and $|i_{dr}| \langle |i_{dr_{ref}}|$. This leads to sudden changes in $|v_{qr}|$ and $|v_{dr}|$. With a high proportional gain, the change in the rotor injected voltage maintains the rotor current below its current limit, thus ensuring continuous operation of the DFIG.

Thus, the operation of the crowbar is mainly determined by the rotor current at the inception and clearance of the fault, which depends on the proportional gain of the controller. Hence, the integral gain component of the controller does not have a material effect on the stability of the DFIG.

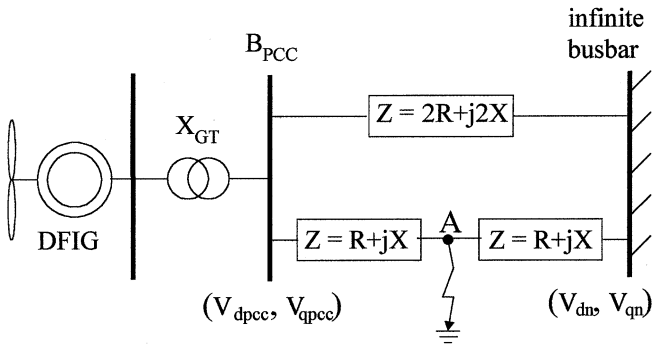

Fig. 4. Network for the fault studies (add $B_{\rm pcc}$).

IV. Simulation Results

The DFIG was simulated using its single-cage and double-cage representation. Appendix A gives the parameters of the 2-MW, 690-V wind generator used for the study.

To investigate the performance of DFIG under system fault conditions, the two-bus double circuit power network shown in Fig. 4 was modeled. At the point of connection of the DFIG ($B_{\rm pcc}$), a short circuit level of 40 MVA with X to R ratio of 5 was used to represent the network connection. The connection transformer was rated at 2.5 MVA and leakage reactance was chosen as 5.9%.

A. Fault Current Contribution and Post-Fault Behavior

For fault studies presented in Figs. 5 and 6, a three-phase fault was introduced at $t = 49.85$ s, with a clearance time of 150 ms. Further, it was assumed that the mechanical input to the turbine was 0.6 p.u.

The fault was introduced at the mid-point of one of the lines (point A) with two values of controller proportional gain settings (K_{P2} of 0.3 and 1.0). The stator current, electromagnetic torque and speed of the machine during the fault and after the fault was cleared is shown in Fig. 5 for $K_{P2} = 0.3$ and Fig. 6 for $K_{P2} = 1.0$. With K_{P2} of 0.3, the crowbar was triggered by the high rotor current when the fault was cleared. However with K_{P2} of 1.0 normal operation of the machine was maintained once the fault was cleared.

Simulations were also carried out with mechanical inputs of 0.4 and 1 p.u. Similar results were obtained.

Fig. 5(a) shows the magnitude of the stator current with both a single cage and double cage rotor representation. When the fault is applied, the double cage model shows a higher initial current peak but a more rapid decay due to the smaller subtransient time constant. The subtransient time constant is approximately 1 ms with the transient time constant around 110 ms. A similar effect can be seen when the fault clears and at this point the over-current protection operates the crowbar circuit. From the simulations, it was found that the rotor current in per unit during the transient is very similar to the stator current.

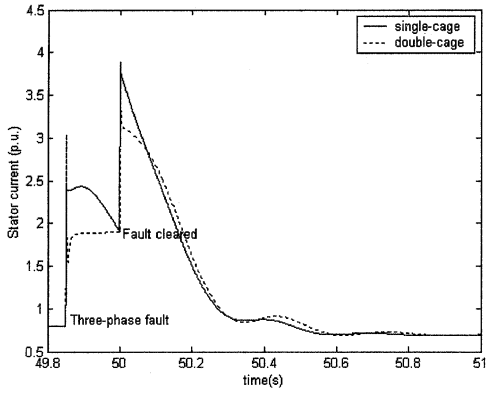

(a)

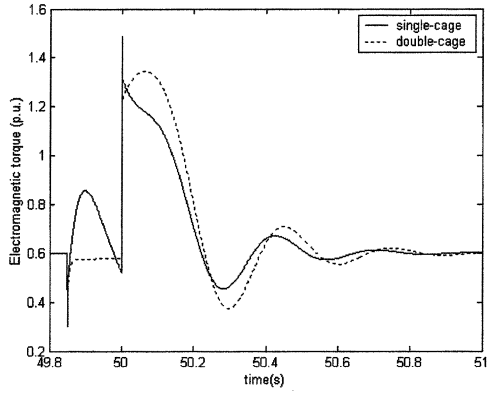

(b)

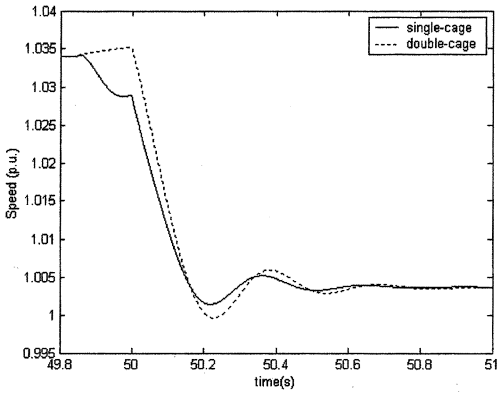

(c)

Fig. 5. For a three-phase fault at the point A of network shown in Fig. 4 with $K_{p2} = 0.3$ and $K_{i2} = 0.5$.

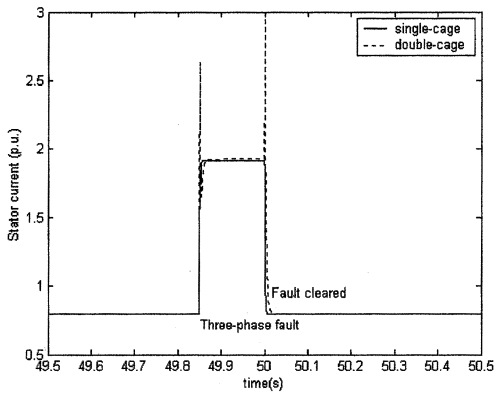

(a)

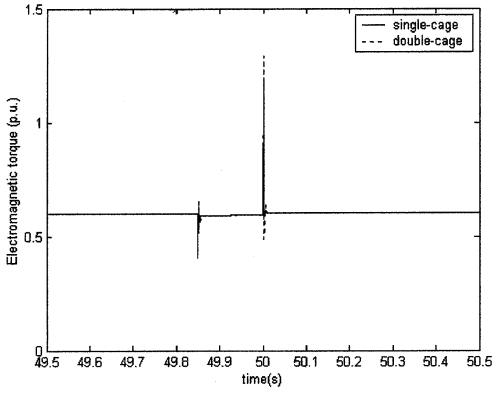

(b)

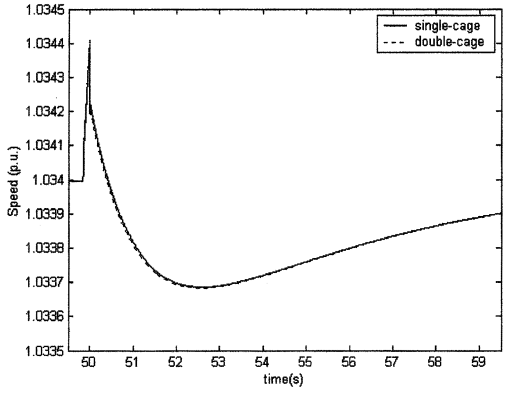

(c)

Fig. 6. For a three-phase fault at the point A of network shown in Fig. 4 with $K_{p2} = 1.0$ and $K_{i2} = 0.5$.

Fig. 5(b) shows the electromagnetic torque, T_e, during the transient. V_{ds} is negligible compared to V_{qs} and so, during the transient T_e mainly depends on i_{qs}, and thus, on i_{qr} [see (8)]. The variation of i_{qr} and hence T_e are determined by the change in rotor speed due to the speed control shown in Fig. 2, and in rotor flux. The variation in rotor flux depend on the single cage and double cage representation.

Fig. 5(c) shows how the operation of the crowbar forces the speed of the machine to near 1 pu (fixed speed operation) although in practice the main generator circuit breaker would be opened once the crowbar operates. The different response of the speed of the machine between 49.85 s and 50 s is due to the different i_{qr} obtained from the single cage and double cage model. As discussed, i_{qr} will act immediately to vary v_{qr} through the effect of the controller.

Fig. 6(a) shows the stator current with the same fault applied but with a higher proportional gain in the controller. The double cage model shows higher sub-transient peak currents but otherwise the response from the two models is very similar. This is because the controller limits the peak currents in both cases. Fig. 6(b) shows the electromagnetic torque, T_e, during the transient. As the change in the rotor speed is very small, T_e mainly depends on the current transients at the inception and clearance of the fault. Fig. 6(c) shows that, during the fault, the speed of the generator is maintained close to its prefault value and returns to normal operation.

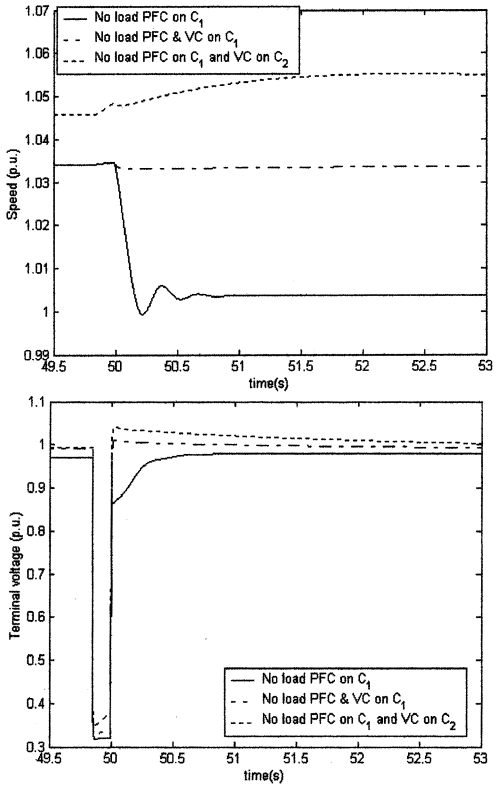

Fig. 7. Network behavior under power factor control (PFC) and VC on different converters.

These simulation results demonstrate the importance of the control system in limiting the generator currents during a fault. Although a double cage model is useful for completeness quite similar results are obtained with the single cage representation. A more important assumption that has been made is that both converters continue to operate normally during and after the fault.

B. Power Factor Control and Voltage Control

The behavior of the wind farm and stability of the associated network depends on the control actions of converters C_1 and C_2. In order to investigate the effect of various control approaches to the behavior of the machine and the network after the fault was cleared, the following three cases were simulated using the DFIG double-cage model. In all three cases the proportional gain of the controller was set low ($K_{P2} = 0.3$).

a) Compensation for the generator magnetising reactive power (No load PFC) was applied through C1.
b) Compensation for the generator magnetising reactive power (No load PFC) and terminal VC were applied through C_1.
c) Compensation for the generator magnetising reactive power (no load PFC) was applied on C_1 and terminal VC on C_2.

The wind farm terminal voltage at the point of connection ($B_{\rm PCC}$) and the generator speed was obtained for all three cases and shown in Fig. 7. In the case of no-load reactive power compensation only, the generator goes unstable following the operation of the crowbar circuit. However, with active voltage control implemented either through C1 or C2, the generator remains stable. There is small difference in terminal voltage, and hence, generator speed depending on whether voltage control is implemented through C1 or C2. This is caused by the different control actions of the two converters (C1 is a voltage source while C2 acts as a current source).

These simulations demonstrate that, as with any synchronous generator, the reactive power control scheme has a significant impact on stability.

V. Conclusions

With increasing wind penetration in power systems, many national grid codes will demand complete models and simulation studies under different system conditions in order to ensure that the connection of a wind farm will not have a detrimental impact on the network to which it will be connected.

Hence a dynamic model with reduced-order double cage representation for the DFIG and its associated control and protection circuits has been developed. It was then used to simulate the response of wind turbine to network faults on a simple two busbar system.

It was demonstrated that by properly selecting the proportional gain of the speed and power factor controller, it is possible to enhance significantly the stability of the DFIG.

Stability was improved using the following techniques: (a) a high proportional gain in the rotor converter limited the rotor current during the fault to a level below the trip setting of the crowbar circuit and (b) fast-acting reactive power control (applied through either converter) improves the stability of the generator.

Voltage control using the rotor side converter (C1) is likely to be preferred to using the network side converter for this task. This is mainly because of the reduction in the converter rating requirement as reactive power injection through the rotor circuit is effectively amplified by a factor of 1/slip.

The models that have been developed are suitable for including in large power system transient stability programs. They include some representation of the practical limitations of the converters (i.e., voltage and current limits) but the representation assumes that the dc link voltage remains constant. This assumption is only valid if the dc link capacitor and converters are designed to enable continued operation of the DFIG with low generator busbar voltages caused by close-up faults.

Appendix

A. 2-MW Induction Wind Turbine Model Parameters (Star Equivalent Circuit)

$V_{base} = 690\,\text{V}, S_{base} = 2\,\text{MW}, \omega_{base} = 2\pi f_{base}, f_{base} = 50$ Hz
Stator resistance (R_s): 0.004 88 p.u.
Stator leakage reactance (X_{ls}): 0.092 41 p.u.
Rotor resistance (R_r): 0.005 49 p.u.
Rotor leakage reactance (X_{lr}): 0.099 55 p.u.
Double-cage resistance (R_d): 0.2696 p.u.
Double-cage reactance (Xl_d): 0.0453 p.u.
Magnetizing reactance (X_m): 3.952 79 p.u.

Rotor to double-cage mutual reactance (X_{rm}): 0.02 p.u.
Lumped inertia constant (H): 3.5 s

B. Control Model Parameters

Cut-in speed $=$ 1000 r/min, Speed limit $=$ 1800 r/min, Shutdown Speed $=$ 2000 r/min.
$K_{opt} = 0.56$, $K_{P2} = 0.3 \& 1.0$, $K_{I2} = 0.5$

ACKNOWLEDGMENT

The authors would also like to acknowledge the contributions of Dr. A. E. Efthymiadis of IPSA Power Ltd.

REFERENCES

[1] S. Muller, M. Deicke, and R. W. De Doncker, "Doubly fed induction generator systems for wind turbines," *IEEE Ind. Applicat. Mag.*, pp. 26–33, May/June 2002.
[2] N. Hatziargyriou, M. Donnelly, S. Papathanassiou, J. A. P. Lopes, M. Takasaki, H. Chao, J. Usaola, R. Lasseter, and A. Efthymiadis, "CIGRE Technical Brochure on Modeling New Forms of Generation and Storage," CIGRE, TF 38.01.10, 2000.
[3] J. G. Slootweg, H. Polinder, and W. L. Kling, "Dynamic modeling of a wind turbine with doubly fed induction generator," in *Proc. IEEE Power Eng. Soc. Summer Meeting*, Vancouver, BC, Canada, July 15-19, 2001.
[4] A. Feijoo, J. Cidras, and C. Carrillo, "A third order model for the doubly-fed induction machine," *Elect. Power Syst. Res.*, vol. 56, pp. 121–127, 2000.
[5] S. S. Kalsi, D. D. Stephen, and B. Adkins, "Calculation of system-fault current due to induction motors," *Proc. Inst. Elect. Eng.*, vol. 118, pp. 201–213, Jan. 1971.
[6] L. Holdsworth, X. G. Wu, J. B. Ekanayake, and N. Jenkins, "Steady state and transient behavior of induction generators (including doubly fed machines) connected to distribution networks," in *Proc. Inst. Elect. Eng. Tutorial "Principles and Modeling of Distributed Generators"*, July 4, 2002.
[7] P. C. Krause, *Analysis of Electric Machinery*. New York: McGraw-Hill, 1986.
[8] P. Kundur, *Power System Stability and Control*. New York: McGraw-Hill, 1994.
[9] V. Akhmatov, A. H. Nielsen, and H. Knudsen, "Electromechanical interaction and stability of power grids with windmills," in *Proc. IASTED Int. Conf., Power and Energy Syst.*, Marbella, Spain, Sept. 19-22, 2000.
[10] R. E. Doherty, "Simplified method of analyzing short-circuit problems," *Trans. Amer. Inst. Elect. Eng.*, vol. 42, p. 841, 1923.

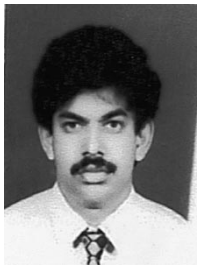

Janaka B. Ekanayake (M'95–SM'02) was born in Matale, Sri Lanka, on October 9, 1964. He received the B.Sc degree in electrical and electronic engineering from the University of Peradeniya, Sri Lanka, in 1990, and the Ph.D. degree in electrical engineering from the University of Manchester Institute of Science and Technology (UMIST), U.K., in 1995.

Currently, he is a Commonwealth and Tyndall Research Fellow with the University of Machester Institute of Science and Technology, U.K. He is a Senior Lecturer in the Department of Electrical and Electronics, University of Peradeniya. His research interests include power electronics, FACTS devices, and renewable energy sources such as wind and small hydro schemes.

Lee Holdsworth was born in England in 1971. He received the B.Eng. (Hons.) and Ph.D. degrees in electrical and electronic engineering from the University of Northumbria at Newcastle, U.K., in 1996 and 2001, respectively.

His industrial experience includes periods with BP Chemicals and BP Oil. Currently, he is a Research Associate with the Manchester Centre for Electrical Energy based at the University of Manchester Institute of Science and Technology, Machester, U.K. His research interests include renewable energy, with particular focus upon wind energy and power electronics applied to power systems.

XueGuang Wu was born in Yunnan, P.R. China, on August 16, 1966. He received the B.Sc degree in electrical engineering from the Northeast Electric Power Institute, China, in 1988, the M.Sc. degree in electrical engineering from Electric Power Research Institute (EPRI) of China in 1996, and the Ph.D. degree in electrical engineering from Wuhan University, China, in 2000.

Currently, he is a Research Associate at MCEE, University of Manchester Institute of Science and Technology, Manchester, U.K., working on integrating renewables and CHP into the U.K. electricity network. His research activities involve electrical power system modeling, system analysis, system control, renewable energy, and embedded generation. He was an Academic Visitor at MCEE, University of Manchester Institute of Science and Technology, working on new and renewable energy technology in 2000.

Nicholas Jenkins (SM'97) received the B.Sc. degree from Southampton University, U.K., the M.Sc. degree from Reading University, U.K., and the Ph.D. degree from Imperial College, London, U.K., in 1974, 1975, and 1986, respectively.

His industrial experience includes periods with Eastern Electricity, U.K., Ewbank Preece Consulting Engineering, U.K., and BP Solar and Wind Energy Group, U.K. He joined the University of Manchester Institute of Science and Technology (UMIST) in 1992 where he is now a Professor and leader of the Electrical Energy and Power Systems Group. His research interests include renewable energy, embedded generation, and FACTS.